Tidal Spectroscopy of the English Channel with a Numerical Model

C. LE PROVOST AND M. FORNERINO*

Institut de Mécanique de Grenoble, C.N.R.S., France

(Manuscript received 15 August 1984, in final form 22 March 1985)

ABSTRACT

The possibility of reproducing the complexity of tides in shallow water areas with a classical finite difference numerical model is examined. This hydrodynamic model is two-dimensional but incorporates topography, nonlinear advection and quadratic bottom friction. Particular care is taken to prescribe sea surface elevations at the open boundaries.

A one-month simulation of "real" tides is run with a simplified spectrum restricted to only 24 constituents, corresponding to the nine main astronomical tides and their nonlinear significant interactions. The results are analysed by spectral decomposition (elevations and vertically integrated currents) and compared with observational data from the tide gages and current meters, and with other solutions produced in the literature.

It is found that:

1) the dominant M_2 constituent greatly influences the damping of the other constituents, so that it is necessary to run them together for any correct simulation; however, the quadratic friction law introduced in the present simulation appears to overdamp these secondary waves by about 5%, without any possible compromise.

2) the nonlinear interaction constituents are remarkably reproduced: for the semidiurnal, quarter-diurnal and six diurnal groups, the precision is within some few centimeters.

3) coherent vertically integrated residual current patterns can be deduced from that simulation, with semimonthly and monthly modulations, which correspond to local nonlinear processes, and to permanent inflow–outflow boundary forcing.

A hindcast of the tidal flow observed at a particular area shows the possibility of using that set of results for tidal current predictions.

1. Introduction

The English Channel is one of the world oceanic regions where tides reach very high values, with sea surface variations greater than 13 m during spring tides in the Bay of Mont St Michel, and currents stronger than 5 m s^{-1} around La Hague Cape. Correlatively the tidal spectrum presents over large areas a very complicated structure. Nonlinear processes taking place within that shallow sea, with depths often less than 50 m, distort waves coming from the ocean, and produce quite atypical profiles, which need a large number of tidal constituents to be correctly parametrized. Several analytical investigations have been developed in the past to understand the basic mechanisms of these distortions. Lamb (1932), using an analytical solution for a long wave propagating in a channel of constant depth, explained how advective terms of the momentum equations and nonlinearity of the continuity equation contribute to steepening of the wave front and lead to bore formation. As tidal bores are unrealistic, Kreiss (1957) investigated the effect of bottom friction by introducing, in the classical nonlinear shallow water equations used by Lamb, a linear friction term proportional to the velocity, and thereby showed the importance of damping. Gallagher and Munk (1971) generalized this approach by using a more accurate quadratic friction term to represent bottom stress; they considered the nonlinear interaction processes occurring between waves propagating simultaneously in the basin. More recently, Kabbaj and Le Provost (1980) demonstrated that such a quadratic bottom friction not only plays a role of damping but also generates nonlinear harmonics that can reach significant amplitudes in shallow waters.

However, all these analytical investigations were limited to schematic channels of constant depth and width. On the other hand, numerical modeling studies over coastal areas have generally been restricted to the main astronomical tidal constituents, M_2, S_2 and K_1, and have not investigated the complete phenomenon including higher harmonics and wave interaction.

The existence of a hydraulic reduced model of the English Channel (Chabert d'Hières, 1962) has made possible an extensive study of the tides over that

* Present affiliation: University of Zulia, Venezuela.

particular area (Le Provost, 1976), leading to the production of a complete set of harmonic charts covering the entire coastal area for 26 tidal constituents: 3 diurnal, 17 semidiurnal, 3 quarterdiurnal and 3 sexto-diurnal (Chabert d'Hières and Le Provost, 1979, hereafter referred to as Ch-LP). Through that particular study, the details of the damping processes of different waves propagating together and the generation of nonlinear constituents over that domain have been clearly understood. The high level of resolution of this tidal spectrum and precision of the results have led to the development of a tidal prediction model based on that collection of cotidal maps (Le Provost, 1981). Comparisons with harbor and offshore tidal gage observations and with satellite altimeter measurements (Le Provost, 1983) have shown that the precision of these predictions is O(10 cm) for tidal ranges of several meters.

That study was unique, however, given the uniqueness of the large rotating physical model used. Thus, a question appeared evidently: is it possible to realize the same kind of detailed investigations with a numerical model, and what will be the precision of the numerical solutions for all significant tidal constituents? The interest of a positive response to that question is evident. If it is so, the same approach can be carried for any coastal area. The results of such a numerical study are also interesting because they must provide not only the tidal elevations but also the tidal currents which are difficult to obtain from a physical model (Fornerino and Chabert d'Hières, 1982).

The aim of this paper is to show that it is possible to obtain a detailed description of tidal elevations and currents within a shallow water domain using numerical modeling. The test area is the English Channel.

2. Brief description of the physics from the observed data

On the northwest European shelf, tides have been observed intensively, leading to a large collection of data, essentially distributed along the coast. Tidal spectra of sea surface elevations are particularly well documented for the French and English coasts of the English Channel. A global view of the importance of different harmonic tidal constituents over that area can be obtained through the diagram presented in Fig. 1, which gives the mean amplitude of the main constituents, computed from ten coastal tide gages. Semidiurnal tides are dominant. The four main constituents are M_2, S_2, N_2, K_2, but we must notice the significant amplitude of L_2, μ_2, ν_2, and even λ_2, which are not purely astronomically induced waves but involve nonlinear semidiurnal interaction waves as listed in Table 1. Quarter-diurnal nonlinear constituents appear also to be quite strong: M_4, the first

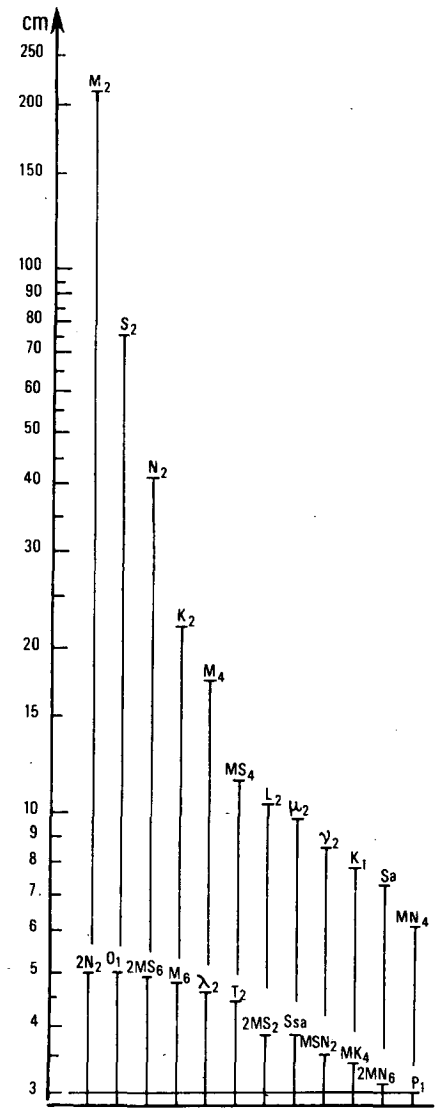

FIG. 1. Order of magnitude of the main tidal constituents over the English Channel; mean amplitude over ten points of observation along the coasts.

harmonic of M_2, MS_4, MN_4 and MK_4, coming from interaction between M_2 and S_2, N_2 and K_2. Even sexto-diurnal waves are very significant: M_6, $2MS_6$ and $2MN_6$. On the contrary, the diurnal constituents do not contribute much to the signal (This is a typical feature of tides within the Atlantic Basin). Such a complex spectrum reflects, in fact, the complicated shape of the tides observed along these coasts, and shows the great interest of using that coastal basin as a test area for the present study. With a numerical hydrodynamic model, we want to reproduce all these constituents over the simulated domain. Its extension will be limited westward at the entrance of the Channel, and eastward just north of the Strait of Dover. Over that area, the astronomical tides can be

TABLE 1. List of the main harmonic constituents of the tides in the English Channel.

Constituent	Angular velocity (deg h^{-1})	Constituent	Angular velocity (deg h^{-1})
Diurnal		Nonlinear semidiurnal	
O_1	13.943 035 6	MNS_2	27.423 833 7
P_1	14.958 931 4	$2MK_2$	27.886 071 2
K_1	15.041 068 6	$2MS_2$	27.968 208 4
		$3MSN_2$	28.512 583 1
Semidiurnal astronomical		SNM_2	29.455 625 3
		$2MN_2$	29.528 478 9
$2N_2$	27.895 354 8	MSN_2	30.544 374 7
μ_2	27.968 208 4	$2SM_2$	31.015 895 8
N_2	28.439 729 5		
ν_2	28.512 583 1	Quarter-diurnal	
M_2	28.984 104 2		
L_2	29.528 478 9	MN_4	57.423 833 7
T_2	29.958 933 3	M_4	57.968 208 4
S_2	30.000 000 0	MS_4	58.984 104 2
K_2	30.082 137 3		
		Sexto-diurnal	
		$2MN_6$	86.407 938 0
		M_6	86.952 312 7
		$2MS_6$	87.968 208 4

considered as waves forced by the oscillations of the open boundaries, freely propagating inside the basin, partly reflected by the bottom and shoreline topography, damped by bottom friction, and distorted by nonlinear shallow water processes, with transfers of energy toward the harmonic and interaction constituents. Thus, the numerical reproduction of that global phenomenon must include exact open boundary condition specifications and correct simulation of the nonlinear processes.

3. The numerical model

a. The hydrodynamic equations

The model is based on the depth integrated shallow water equations, which can be written, under some assumptions (Nihoul, 1975; and Johns, 1983):

$$\left.\begin{aligned} &\frac{\partial \mathbf{U}}{\partial t} + \nabla(H^{-1}\mathbf{U}\mathbf{U}) + f\mathbf{k}\times\mathbf{U} \\ &\qquad = -\gamma H\nabla\zeta - \frac{D}{H^2}|\mathbf{U}|\mathbf{U} + \nu_0\nabla^2\mathbf{U} \\ &\frac{\partial \zeta}{\partial t} + \nabla\cdot\mathbf{U} = 0 \end{aligned}\right\} \quad (1)$$

with

$$\left.\begin{aligned} &\mathbf{u} = u\mathbf{i} + v\mathbf{j} \\ &\mathbf{U} = \int_{-h}^{\zeta}\mathbf{u}\,dz, \quad \mathbf{U} = U\mathbf{i} + V\mathbf{j} \\ &H = h + \zeta \end{aligned}\right\}$$

where we denote by

- **i, j, k** the unit orthogonal vectors of a reference system (x, y, z), tangent to the geoid at the center of the studied area $\mathcal{D}$, with x and y axis respectively eastward and northward and z axis vertically upward.
- ζ the elevation of the sea surface above the undisturbed level
- h the still-water depth
- u, v the eastward and northward components of current
- U, V the corresponding depth integrated transport components
- D the bottom drag coefficient
- ν_0 the horizontal subgrid scale dissipation parametrization
- f the Coriolis parameter set equal to a constant
- γ the gravitational acceleration.

The coastal boundary condition is no normal flow:

$$\mathbf{U}\cdot\mathbf{n} = 0 \quad \text{along} \quad \Gamma_C \qquad (2a)$$

A choice of conditions is available for open sea boundaries:

1) to specify elevation as a function of position and time

$$\zeta = \zeta_0 \quad \text{along} \quad \Gamma_0 \qquad (2b)$$

2) to specify a relationship between elevation and transport, expressing some "radiation condition." Such a condition reduces artificial reflection from the open boundary, when direct prescription of ζ_0 along Γ_0 is not possible because of lack of observed data, or not well adapted to the modeled dynamics. (see Flather, 1976).

In the present work, type (2b) open boundary condition is used because a very accurate $\zeta_0(\Gamma_0, t)$ distribution can be supplied by reference to the previous studies of Ch-LP.

b. The finite difference discretization

The domain of simulation is presented in Fig. 2. It is limited westward and eastward by two open boundary lines, AB and CD. The grid of computation has a uniform spacing of 10 km. The variables are staggered in space, following the grid scheme presented in Fig. 2. Batten and Han (1981) have shown recently that for linearized shallow water equation, that grid introduces smaller numerical noise. Depths over the network were deduced from bathymetric charts of the Channel. Values lower than 5 m have been arbitrarily set to 5 m to avoid "drying" areas and uncontrolled divisions by zero in the model code, connected to the bottom friction law used in (1).

The numerical scheme is a predictor–corrector and is summarized as follows. By separating time deriva-

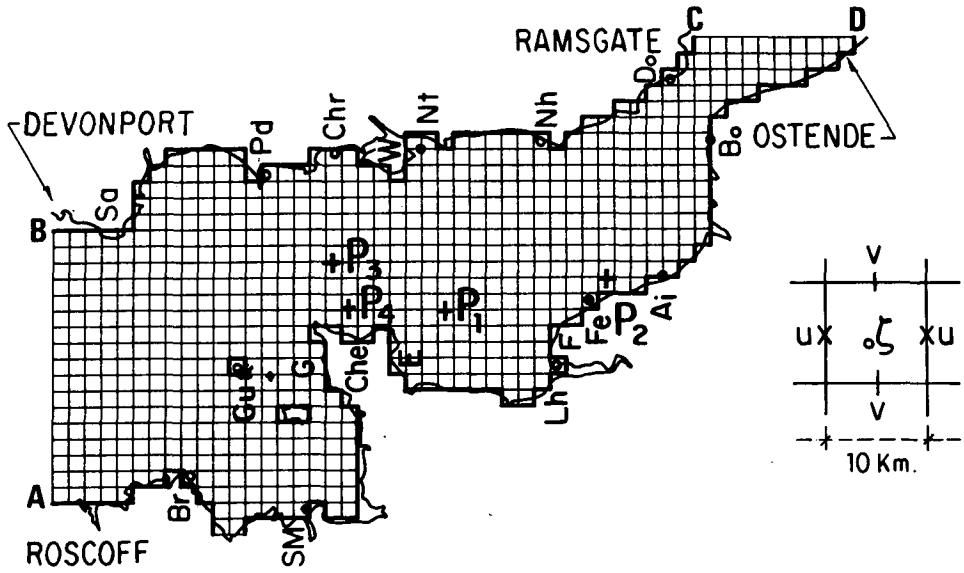

FIG. 2. The English Channel. The model extension and the computational grid. Typical locations are E: Barfleur Cape, F: Bruneval, G: La Hague Cape, H: Mont St Michel Bay, W: Isle of Wight, Br: Bréhat Island, SM: St Malo, Gu: Guernesey Island, Che: Cherbourg, Lh: Le Havre, Fe: Fécamp, D: Dieppe, Bo: Boulogne, Do: Dover, Nh: New Haven, Nt: Nab Tower, Chr: Christchurch, Pd: Portland Sa: Salcomb.

tives from the rest in system (1), one can write these equations as:

$$\left.\begin{aligned}\frac{\partial \mathbf{U}}{\partial t} &= \mathbf{f}_D(\mathbf{U}, H, \zeta)\\ \frac{\partial \zeta}{\partial t} &= f_C(\mathbf{U})\end{aligned}\right\} \tag{3}$$

where $\mathbf{f}_D$ is a function of $\mathbf{U}$, H, and ζ and their space derivatives, and f_C, of $\mathbf{U}$ and its derivatives. The numerical integration proceeds in two steps:

1) Starting from time t, an estimate of the unknown variables at $t + \Delta t/2$ is first computed through an upstream space derivative scheme:

$$\left.\begin{aligned}\mathbf{U}_{t+\Delta t/2} &= \mathbf{U}_t + \frac{\Delta t}{2}\mathbf{f}_D{}^{\mathrm{UP}}(\mathbf{U}_t, H_t, \zeta_t)\\ \zeta_{t+\Delta t/2} &= \zeta_t + \frac{\Delta t}{2} f_C{}^{\mathrm{UP}}(\mathbf{U}_{t+\Delta t/2})\end{aligned}\right\} \tag{4}$$

2) The new solution at $t + \Delta t$ is then computed from the solution at t with centered space derivatives but at the intermediate $t + \Delta t/2$ time step:

$$\begin{aligned}\mathbf{U}_{t+\Delta t} = \mathbf{U}_t + \Delta t[&\mathbf{f}_D{}^{\mathrm{CE}}(\mathbf{U}_{t+\Delta t/2}, H_{t+\Delta t/2}, \zeta_{t+\Delta t/2})\\ &+ \alpha\nabla^2\mathbf{U}_{t+\Delta t/2}]\\ \zeta_{t+\Delta t} = \zeta_t + \Delta t f_C{}^{\mathrm{CE}}&(\mathbf{U}_{t+\Delta t/2}).\end{aligned} \tag{5}$$

The first half time step, the predictor step, is unconditionally stable, but diffusive and of first order only, in precision (Richmeyer and Morton, 1967), the second, the corrector time step, is *a priori* unstable, and needs some additional viscosity $\alpha\nabla^2\mathbf{U}$ to be stabilized.

It must be noticed that a purely diffusive scheme is not adequate for our purpose, which is to reproduce, in particular, the nonlinear advective processes. We know (Roache, 1972) that when such a scheme is used, uncontrolled and artificial damping of short waves can occur which affect the transfer of energy from the main constituents to higher harmonics. Indeed, some preliminary tests have shown that the M_4 constituent, for instance, cannot be obtained correctly over the Channel with a diffusive scheme (Ronday, 1977). On the contrary, as we shall see later, this predictor–corrector scheme, which is globally of second-order precision in space and time, can give very satisfying solutions. As we are explicit in time, the Courant-Friedrichs-Levy condition must be applied:

$$\Delta t \leqslant \Delta x/\{[2\gamma(H + \zeta)]^{1/2} + u\}_{\max}$$

which imposes, given the grid size and the depths and velocities over $\mathcal{D}$, a maximum time step of the order of 190 s. We have taken $\Delta t = 184.009$ s, which gives us exactly 243 time steps per lunar M_2 period.

c. *The initial and boundary conditions*

The computations start from rest ($\zeta = 0$, $\mathbf{U} = 0$), and the tidal oscillation is progressively spun up inside the domain through the open boundary forcing, where sea surface elevations are prescribed, following:

$$\zeta_0(M) = \zeta_m(M) + \sum_{i=1}^{N} A_i(M) \cos[\omega_i t + \vartheta_i - g_i(M)] \quad (6)$$

with the notations:

$\zeta_m(M)$	mean sea level, referred to the geoid, at point M
N	number of tidal constituents included in the simulation
$A_i(M), g_i(M)$	amplitude and phase of component i at point M
ω_i	frequency of constituent i
ϑ_i	phase of equilibrium i constituent at time $t = 0$ at GMT.

It has been experimentally observed that it takes four semidiurnal periods before friction and boundary forcing remove the influence of initial conditions.

The use of open boundary condition of (2b) type has been possible in the present application because of the particular care taken to define the sea surface elevation along Γ_0, by referring to the already known solutions of Ch-LP. Since advective and horizontal viscosity terms are included in the numerical model, it is necessary to prescribe another boundary condition besides the coastal condition of no normal flow. Given the size of the grid ($\Delta x = \Delta y = 10$ km), we have used a slip condition.

4. Initial tests of the model

Some preliminary tests have been done, which are interesting to present briefly because they give some insights in the physics of the phenomenon. In order to save computer time, and also for simplicity, these tests have been conducted with the M_2 tide, and its nonlinear constituents M_4 and M_6. The main sensitivity studies were concerned with bottom damping, horizontal eddy viscosity, and open boundary conditions.

a. The boundary conditions

With the present limitations, formula (6) reduces to three constituents, so that we have to prescribe ζ_m, ζ_{M_2}, ζ_{M_4}, ζ_{M_6} and g_{M_2}, g_{M_4}, g_{M_6} along the open boundaries AB and CD. Observed data are available at points A (Roscoff), B (Devonport), C (Ramsgate) and D (Ostende), and the distributions between these points are already known from previous studies of Ch-LP (1979), who gave the spatial distribution of these parameters over the Channel. In order to illustrate the importance of the correct choice of open boundary conditions, we have compared the response of the model to three typical situations:

Run E1: most realistic distribution, deduced from Ch-LP.

Run A1: linear distribution along AB and CD computed at each time step from $\zeta_A(t)$ and $\zeta_B(t)$, $\zeta_C(t)$ and $\zeta_D(t)$

Run A2: The same as E1, but without any M_4 and M_6 contribution.

The main results are the following:

1) The two hypothesis E1 and A1 introduce only a small deviation between the prescribed elevations ζ_{M_2} along the Atlantic open boundary (maximum difference 4 cm, i.e., 2%). Consequently little differences are observed inside the domain for the M_2 constituent. (maximum deviation 3 cm).

2) On the contrary, the differences are significant for the first harmonic. The A1 hypothesis introduce a discrepancy of 20% on M_4 along AB, which gives a deviation of 13% in the Bay of Mont St Michel: this is due to the particular distribution of that constituent through the entrance of the Channel. Experiment A2 illustrate even more clearly the importance of a good prescription of that constituent along the open boundary. The corange lines of that solution are presented in Fig. 3 which is to compare with E1 (Fig. 6). We will comment further on the quality of the E1 solution with the two amphidromic points in the western and the eastern basins. But it is surprising to discover that in the A2 experiment, the western amphidromic point completely disappears. In fact, a zero value of M_4 along the open boundaries of the model is physically wrong. The ζ_{M_4} needs to be prescribed very correctly along the open boundaries.

3) Nothing significant is observed for the M_6 constituent, principally because that wave presents very small amplitudes along the open boundaries.

It appears through the present test that the precision of the solution inside the domain can be dramatically dependent of the correctness of the boundary conditions. In the following, we will use the best possible set of data, which will be deduced from Ch-LP.

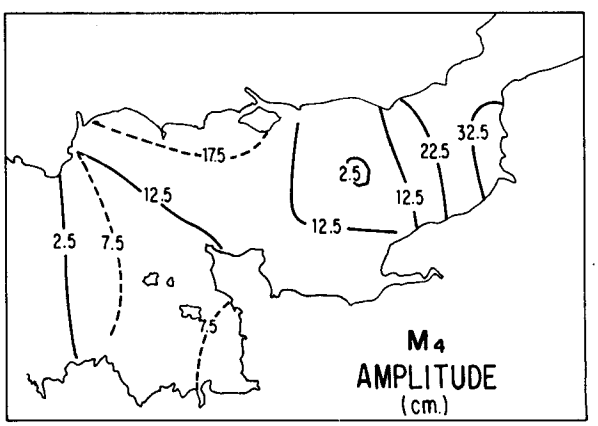

FIG. 3. M_4 corange solution with zero M_4 amplitude prescribed along the open boundaries AB and CD.

b. The bottom damping

Several values of the bottom friction coefficient D have been tested, ranging from 2.0 to 2.8 ($\times 10^{-3}$). In all the cases, we have restricted ourselves to some unique value, although better improvements could be achieved by using spatially varying optimized coefficients. It appears that a decrease of bottom friction of the order of 13% improves the solution in the eastern basin of the order of 4% for M_2 and 13% for M_4. Surprisingly, it does not modify M_2 in the Bay of Mont Saint Michel (near St. Malo), although the depths are very shallow in that area. On the contrary, the M_4 solution is reduced over that area. (These features are difficult to interpret physically, as far as the boundary conditions are kept constant for the different simulations.) A detailed check of the numerical results with available coastal data leads to the conclusion that $D = 0.0023$ give the best results.

c. The horizontal diffusion coefficient

Very often, classical tidal models over coastal areas do not use any horizontal diffusion term. We have noticed previously that, with the predictor–corrector scheme, some numerical viscosity is at least necessary for stability of the computations. However, the value needed is quite small. Given the maximum velocity expected over the modeled area and the time step, the numerical viscosity coefficient α can be estimated of the order of 100 $m^2\ s^{-1}$.

The English Channel is an area where important velocities and velocity gradients can be observed around capes. The horizontal viscosity can play a significant role there. In context of the present numerical model, we have an opportunity to investigate some physically significant contributions of the horizontal eddy diffusion term $\nu_0\nabla^2 U$, by checking our solution with *in situ* observations in the vicinity of Barfleur Cape. Along a section EF (see Fig. 2), we have four observed data points, E (Barfleur harbour), F (Bruneval harbour), and two bottom sea tide gages (Bertherat *et al.*, 1981). We have thus tested different values of $\nu = \nu_0 + \alpha$. It is possible to find several combinations for (D, ν) giving the same overall quality for the M_2 solution, but we can improve that solution around capes by increasing the horizontal eddy viscosity ν. As an illustration, we present the results from two sets of coefficients (see Fig. 4).

Run E1: $D = 0.0023$ and $\nu = 5000\ m^2\ s^{-1}$
Run E3: $D = 0.0028$ and $\nu = 1000\ m^2\ s^{-1}$.

Around Barfleur, better results are obtained by increasing ν; horizontal diffusion must play an important role locally. In the framework of the present numerical formulation, with a constant grid size of 10 km and slip boundary conditions along the coast line, the ideal solution would be to adopt a variable ν coefficient taking larger values over particular areas

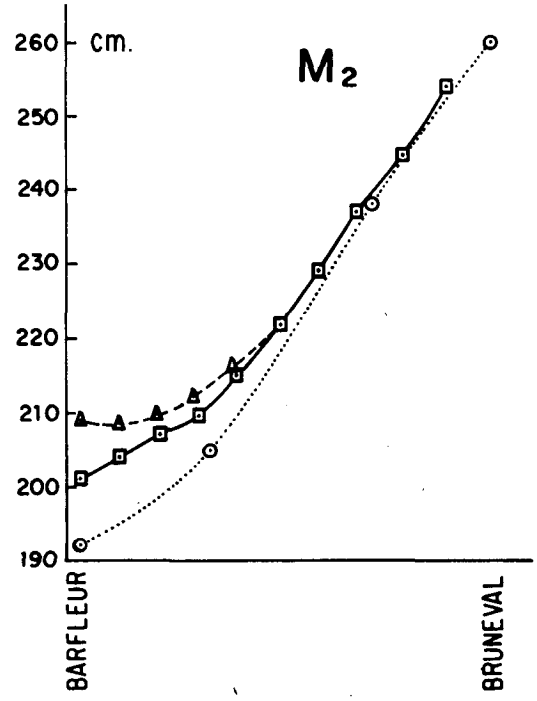

FIG. 4. Comparison of the M_2 solution with observations in the vicinity of Barfleur Cape, along the line EF Barfleur-Bruneval. (Squares) Run E1: $D = 0.023$, $A = 5000\ m^2\ s^{-1}$; (Triangles) Run E2: $D = 0.028$ $A = 1000\ m^2\ s^{-1}$; (Circles) observed.

where important velocity gradients occur. Even better improvements could be obtained, of course, by using variable grid sizes refining the meshes around the capes, and allowing a no-slip condition at the coast line. But for the present work, we have retained for future investigations the E1 set of coefficients.

As we shall explain later, the M_6 solutions is not good, in any case, for that class of simulation with M_2 alone. However, it must be noticed that the solution is somewhat improved by increasing ν. We do not comment on the results for the M_4 constituent, because no significant difference appears between these different tests.

d. Global checking of the best fit to observations

The cotidal and corange maps for M_2 and M_4 are presented in Figs. 5 and 6.

The M_2 solution is very classical, with a virtual amphidromic point inland, south of England, at the midlongitude of the basin, and a local increase of amplitude up to 4 m in the Bay of Mont Saint Michel due to reflection of the eastward incoming tidal wave along the north–south coast of Cotentin peninsula. The cotidal lines are also typical of a Kelvin amphidrome, rotating counterclockwise around the virtual amphidromic point. It can be seen in Fig. 7 that the solution fits quite well to the observations even for a 10 km mesh model. The mean deviation over the

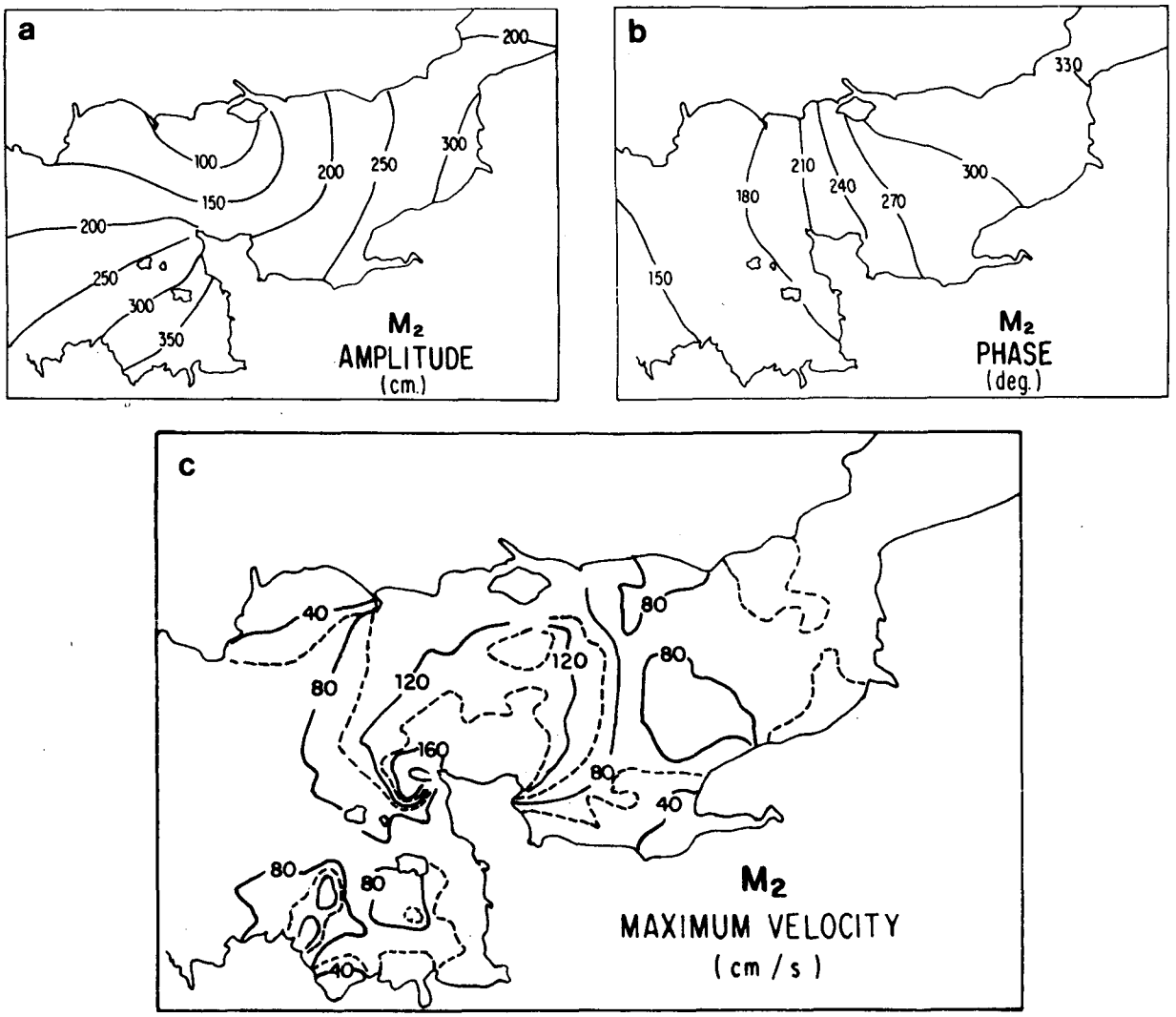

FIG. 5. Semidiurnal M_2 solution of (a) amplitude (cm), (b) phase g (deg) of the sea surface elevation and (c) amplitude (cm s^{-1}) of the velocity field.

nine points of comparison used along the French coast is 6.6 cm in amplitude and 4° in phase. Along the English coast, the solution is a little less perfect, with a mean deviation of 9.9 cm in amplitude and 10° in phase over 15 points of comparison. The solution is too strong, especially between Portland and Nab Tower, i.e., in the vicinity of the amphidromic point which is effectively a difficult area to reproduce correctly, as a small discrepancy between the incoming eastward and the reflected westward waves introduce a significant shift of the amphidromic point, and thus systematic errors in amplitudes and phases. However, this solution can be considered satisfactory. As seen in Sections 4b and 4c it could be refined by adjusting locally the D and ν parameters, but our aim is not to go further here in that way of refinement. We are more interested in the nonlinear interactions, particularly reflected through the higher harmonics.

The M_4 solution can be also compared favorably to the observations. This wave presents two real amphidromic points, at 3°W and 0°, and areas of maxima up to 35 cm in the Bay of Mount St Michel and near Boulogne, which corresponds to 10% of the M_2 amplitude over these areas. Similar solutions have already been produced by Ch-LP (1979) using their physical reduced model of the channel, and Pingree and Maddock (1978) with a numerical model. It must be noticed that the phase propagations of that component indicate that an important part of the M_4 energy is radiating from the central part of the domain between 0° and 2°W, which proves that a transfer of energy from the M_2 frequency to the M_4 frequency is occuring in that area, through nonlinear

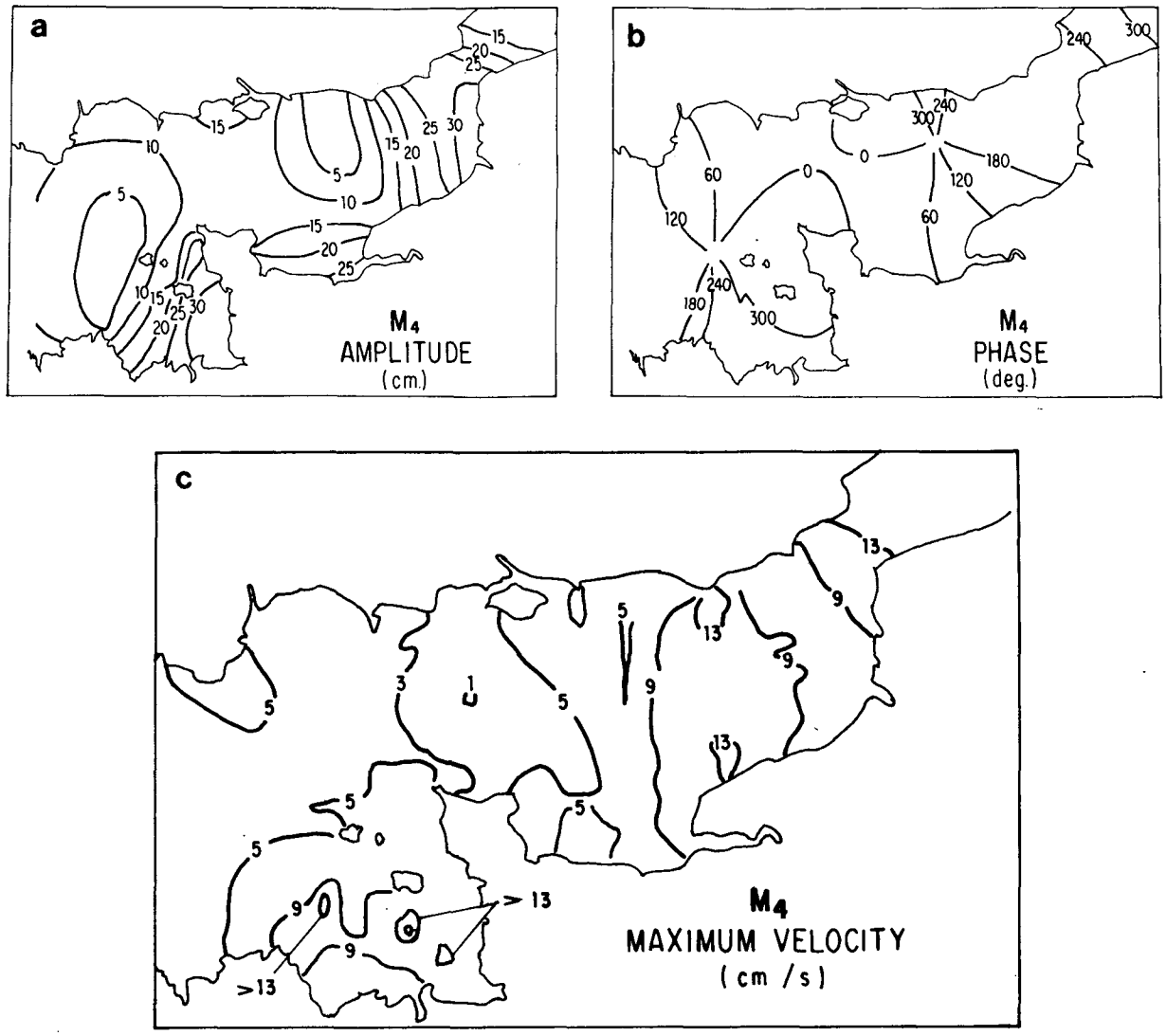

FIG. 6. As in Fig. 5 but for quarter-diurnal M_4 solution.

processes. As we shall see later, in this central part of the Channel, the currents reach large values, with important gradients around the different capes (La Hague, Barfleur, St. Catherine).

We do not present here the M_6 constituent because of lack of space. The results are qualitatively the same as produced by Ch-LP (1979) for that component, with complicated cotidal and corange maps because of the smallness of the corresponding wave length (typically about 300 km). The main features are a nodal line joining Dieppe, New Haven, Barfleur, Guernesey and Salcombe, and areas of maxima around Christchurch, Le Havre, and the strait of Dover. However, the important thing to notice here is that this E1 run gives too large amplitudes for the M_6 constituent, by about 35%. We shall see later how to correct that systematic discrepancy and explain it.

5. Design of a monthly simulation

As noticed in Sections 1 and 2, tidal waves are very energetic in the English Channel so that strong nonlinear interactions occur between these components through hydrodynamic and damping processes. In order to reproduce and analyse these interactions, we designed a simulation involving a large number of constituents. Given the complexity of the real spectrum, and the importance of the prescription of the boundary conditions (cf. Section 4a), particular care must be taken for the choice of the constituents to be introduced at the open limits of the model. On the other hand, we have seen that the main parameters to be adjusted in the model are the damping coefficients; new coefficients must be chosen for the present simulation, and we shall see how to deduce them

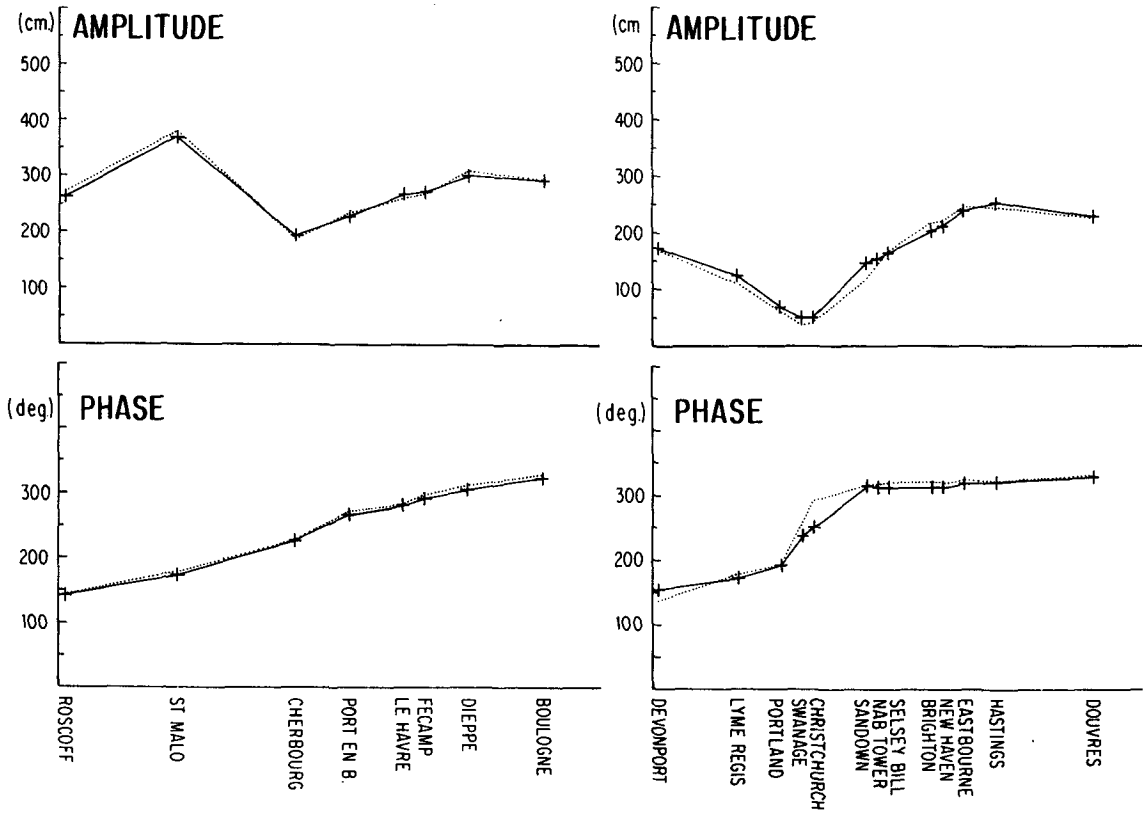

FIG. 7. Comparison of the E1 numerical solution (solid line) with observations (dotted line) along the coasts of the English Channel.

from the previous runs without any trial and error procedure (which would be very expensive for long simulations).

a. The constituents introduced in the simulation

Figure 1 illustrates the complexity of the tidal spectrum over the studied area. More than 24 constituents are significant and interact between each other. To be fully satisfying, our simulation would involve all these waves. However, we must take care of the well known difficulty of tidal signal analysis (long time series of observations are needed to clearly separate the neighboring frequencies). It will be the same for the harmonic analysis of our numerical results. Thus, a reproduction of the complete spectrum implies a very long simulation, of the order of six months or one year, to be able to separate secondary waves like K_2 and T_2 from S_2, and this becomes computationally time consuming.

In order to limit computer costs, we have designed a simplified simulation giving the possibility to analyse and separate all the contributive frequencies introduced in the simulation. The typical modulations of the tidal signals are semimonthly, monthly, semiannual and annual. One month appears as a reasonable time scale for our purpose. All the main astronomical constituents can be taken into account in such a simulation, except the declinational K_2. We have thus decided to do so, and investigate a simplified spectrum selected as follows.

For astronomical waves, in each species the major constituents of each separable band are retained:

Semidiurnal: ϵ_2, μ_2, N_2, M_2, L_2, S_2

Diurnal: Q_1, O_1, K_1

We eliminate from the real spectrum the secondary waves $2N_2$, ν_2, λ_2, T_2 and K_2, in the semidiurnal, and P_1 in the diurnal species, which cannot be separated over one month from respectively μ_2, N_2, L_2, S_2 and K_1.

Given that simplified astronomical spectrum, and by reference to what can be qualitatively assumed from our knowledge of nonlinear interaction processes (cf. Le Provost, 1976), the following list of nonlinear constituents must be taken into account,

long period:	Msf, Mf corresponding to interactions M_2–S_2 and M_2–N_2
diurnal:	no significant contribution

semidiurnal:	$2MS_2$ (mixed with μ_2), and $2SM_2$ for M_2–S_2 interactions
	$2MN_2$ (over L_2) for M_2–N_2 interactions
	MNS_2 (over ϵ_2) and MSN_2 for M_2–S_2–N_2 interactions
	$3MSN_2$ and SNM_2 (which will introduce some difficulties in the analysis, because of their proximity to N_2 and L_2)
quarter diurnal:	M_4, MS_4 and MN_4
sextor-diurnal:	M_6, $2MN_6$, and MSN_6.

This selection gives 24 constituents which must be prescribed along the open boundaries following (6). For the Atlantic limit AB, an empirical distribution of the amplitudes and phases have been established from the atlas of Ch-LP (1979). As noticed in Section 4a, a similar set of data could have been established by a linear interpolation from observed data in Roscoff and Devonport, except for the quarter-diurnals. For the CD North Sea limit, a linear interpolation between Ostend and Ramsgate has been used, given the lack of knowledge along that boundary. Some tests have been done to verify that solutions inside the English Channel are not too sensitive to that approximation.

With this simplified spectrum, numerical computations were performed over one month. An example of sea surface variations is presented in Fig. 8. It can be noticed that semimonthly and monthly modulations are clearly produced and that the simulation starts from mean spring tides. Similar time series were obtained for sea surface elevations and current components at all u or v points of computation.

b. *The bottom friction coefficient used*

The simplified simulation used for preliminary tests of Section 4, reproducing M_2 alone, was performed with $D = 0.0023$, which is a classical value. As we have noticed when comparing this solution with the observations, the results of that approximation are surprisingly good, given the fact that tidal damping is not only a function of the M_2 energy level, but also of all significant constituents in the spectrum. The explanation can be found through the spectral analysis of the bottom friction terms $|U|U$ established analytically by Le Provost (1973). Studying the damping bottom friction terms,

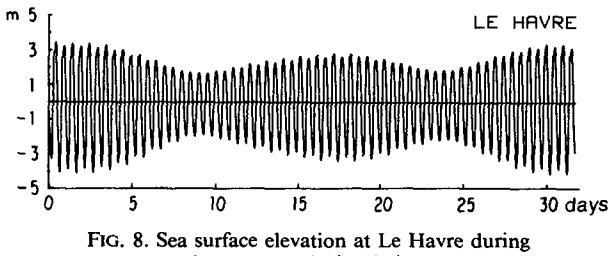

FIG. 8. Sea surface elevation at Le Havre during the one-month simulation.

$$F_x = D(U^2 + V^2)^{1/2}U$$
$$F_y = D(U^2 + V^2)^{1/2}V, \quad (7)$$

and considering that the solution can be developed in the form

$$U = \sum A_i U_i \cos(\omega_i t + \phi_{U_i})$$
$$V = \sum A_i V_i \cos(\omega_i t + \phi_{V_i}), \quad (8)$$

with A_i characterizing the amplitude of the ith wave, an approximate Fourier development of (7) can be obtained, when one tidal constituent (i.e., M_2 taken as index 1) is of much greater amplitude than the others in the spectrum. The result is

$$\begin{aligned} F_x/D = {} & A_1^2 \sum_n FX_{11}^{(n)} \cos[(2n+1)\omega_1 t + \phi X_{11}^{(n)}] \\ & + A_1 A_j \sum_{n,\epsilon} FX_{1j}^{(n,\epsilon)} \cos[(2n\omega_1 + \epsilon\omega_j)t + \phi X_{1j}^{(n,\epsilon)}] \\ & + A_j^2 \sum_{n,\epsilon,\delta} FX_{jj}^{(n,\epsilon\delta)} \cos\{[(2n+1)\omega_1 + 2\epsilon\delta\omega_j]t \\ & + \phi X_{jj}^{(n,\epsilon\delta)}\} + A_j A_S \sum_{n,\epsilon,\epsilon'} FX_{js}^{(n,\epsilon,\epsilon')} \cos\{[(2n+1)\omega_1 \\ & + \epsilon\omega_j + \epsilon'\omega_s]t + \phi X_{js}^{(n,\epsilon,\epsilon')}\} + \cdots, \end{aligned} \quad (9)$$

with a similar development for F_y. Here $n = 0, 1, 2, \ldots, \epsilon$ and $\epsilon' = \pm 1$, $\delta = 0$ or 1 and FX, FY, ϕX, ϕY are functions of U_i, V_i, ϕ_{U_i} and ϕ_{V_i}. These functions have been determined analytically for the orders A_1^2, $A_1 A_j$ and A_j^2.

When applied to the dynamics of tides over the European continental shelf, the different terms of (9) contribute to the following frequencies,

terms A_1^2:	M_2 ($n = 0$), M_6 ($n = 1$), $\cdots$
terms $A_1 A_j$:	$S_2, N_2, K_2, \ldots$, ($n = 0$)
	$2MS_2, 2MN_2, 2MK_2, \ldots$, ($n = 1$, $\epsilon = -1$)
	$2MS_6, 2MN_6, 2MK_6, \ldots$, ($n = 1$, $\epsilon = +1$)
terms A_j^2:	M_2 ($n = 0$, $\delta = 0$), M_6 ($n = 1$, $\delta = 0$)
	$2SM_2, 2NM_2, \ldots$, ($n = 0$, $\delta = 1$, $\epsilon = +1$)
	$2SM_6, 2NM_6, \ldots$, ($n = 0$, $\delta = 1$, $\epsilon = -1$)
terms $A_j A_s$:	$MSN_2, MNS_2, MSK_2, \ldots$, ($n = 0$, $\epsilon = +1$, $\epsilon' = -1$)
	$MSN_6, MNS_6, MSK_6, \ldots$, ($n = 0$, $\epsilon = +1$, $\epsilon' = +1$).

Some comments can be given when looking at these results. For $n = 0$, (9) gives the basic frequencies ω_1 and ω_j, and the corresponding terms represent the damping role of the bottom friction. In this case, (9) suggest new frequencies ($2\omega_1 - \omega_j$, $2\omega_1 + \omega_j$, $3\omega_1$, $5\omega_1$, $\cdots$), which corresponds to the generation by bottom friction of new nonlinear constituents such

as $2MS_2$, $2MS_6$, M_6, $M_{10}\cdots$. We shall see later the importance and the aspect of these waves over the English Channel.

It is important to notice in the context of the present multiperiodic simulation, that the M_2 frequency (ω_1) appears in (9) at the orders A_1^2 and A_j^2 only (for $n = 0$ and $\delta = 0$). Consequently, F_x and F_y can be written for the M_2 damping as follows:

$$\left.\begin{aligned} F_x(\omega_1) &= D[A_1^2 FX_{11}^{(0)} \cos(\omega_1 t + \phi X_{11}^{(0)}) \\ &\quad + \sum_j A_j^2 FX_{jj}^{(0,0)} \cos(\omega_1 t + \phi X_{jj}^{(0,0)})] \\ F_y(\omega_1) &= D[A_1^2 FY_{11}^{(0)} \cos(\omega_1 t + \phi Y_{11}^{(0)}) \\ &\quad + \sum_j A_j^2 FY_{jj}^{(0,0)} \cos(\omega_1 t + \phi Y_{jj}^{(0,0)})] \end{aligned}\right\}. \quad (10)$$

Development (10) shows that the M_2 damping is produced not only by the M_2 bottom friction but also by a contribution from all other main components in the spectrum.

Although the general analytical formulations of the functions FX, FY, ϕX and ϕY are complex (see Le Provost, 1974; Kabbaj and Le Provost, 1980), they can be considerably simplified when the spectrum is reduced to the main semidiurnal constituents (M_2, S_2, N_2, L_2, μ_2), because of the similarities between these different waves, in amplitude and phase. With the hypothesis that the amplitudes of the different constituents are in the same ratio from wave to wave, everywhere over the studied area, and that their phases are linearly related [for example, see the relations (15) and (16) in the following], (10) can be simplified to the form

$$F_x(\omega_1) = D \cos(\omega_1 t + \phi) A_1^2 FX_{11}^{(0)} \times \left\{1 + \sum \left(\frac{A_j}{A_1}\right)^2 \frac{FX_{jj}^{(0,0)}}{FX_{11}^{(0)}}\right\}, \quad (11)$$

with $FX_{jj}^{(0,0)}/FX_{11}^{(0)} \approx 0.75$, i.e.

$$F_x(\omega_1) = D \cos(\omega_1 t + \phi) A_1^2 FX_{11}^{(0)} \times \left\{1 + 0.75 \sum \frac{A_j^2}{A_1^2}\right\}. \quad (12)$$

Approximation (12) explains why the simplified simulation of M_2 alone has been able to give a correct solution, by taking a D_{M_2} damping coefficient equal to the real D multiplied by the coefficient

$$1 + 0.75 \sum (A_j/A_1)^2$$

which artificially compensates for the absence of damping introduced in the real phenomenon by the presence of the other semidiurnal waves in the spectrum (S_2, N_2, K_2, L_2, μ_2). If we take the main numerical values of the characteristic A_j from Fig. 1, we obtain for the present simulation a practical value of

$$1 + \frac{0.75}{A_{M_2}^2}\{A_{S_2}^2 + A_{N_2}^2 + A_{L_2}^2 + A_{\mu_2}^2 + A_{\epsilon_2}^2\} = 1.128. \quad (13)$$

The damping coefficient D used for the monthly simulation has been taken consequently as 0.0023/1.128 = 0.00204, and we shall see in the following that this is effectively a good value.

c. *Methodology for the analysis of the results*

At every point of computation over the domain, a time series is obtained for ζ, u or v. As we want to identify the ability of the model to correctly reproduce the details of the different nonlinear transfers of energy from the incoming oceanic waves to the harmonic and interaction constituents observed in nature, we have to express these time series in the form of harmonic developments,

$$S(t) = S_m + \sum_{i=1}^{N} [S_i \cos(\omega_i t - g_i)] + \epsilon(t). \quad (14)$$

This can be done following a classical harmonic analysis mean square method (cf. Shureman, 1958; Godin, 1972). It must be noticed that the selection of waves introduced *a priori* in the simulation has been established so as to have no problems of harmonic analysis (see Section 5a). However, some particular comments are necessary concerning the existence in the simulated spectrum of three mixed waves and of two nonlinear waves very close to other waves already induced by the boundaries.

1) THE MIXED WAVES

Three pairs of constituents need to be considered carefully:

μ_2 and $2MS_2$, L_2 and $2MN_2$, ϵ_2 and MNS_2.

Each constituent in the pair has the same frequency but they are of different origin (astronomical or nonlinear). Consequently they must present significant hydrodynamic differences. The former are induced inside the domain by the boundaries only, and the latter are partly generated inside the modeled area by nonlinear distorsions and interactions of the main constituents during their propagation over shallow water. As these pairs have exactly the same frequency, the harmonic analysis gives only the sum of the two, which is then physically difficult to interpret. We have thus decided to separate them by stating *a priori* that the astronomical components μ_2, ϵ_2 and L_2 are very similar to the neighboring N_2 and M_2 and that they can be deduced from them by linear interpolations. For μ_2, as example, the amplitudes and the phases are taken as:

$$A_{\mu 2} = A_{N_2} \times \frac{C_{\mu 2}}{C_{N_2}} \tag{15}$$

$$g_{\mu 2} = g_{N_2} + \frac{\omega_{\mu 2} - \omega_{N_2}}{\omega_{M_2} - \omega_{N_2}} (g_{M_2} - g_{N_2}) \tag{16}$$

with $C_{\mu 2}$, (C_{N_2}) tidal potential coefficient for μ_2, (N_2).

This can be approximately verified for most of the semidiurnal constituents over limited areas such as the English Channel. (Le Provost, 1974). Consequently, by difference, the amplitude and the phases of the nonlinear corresponding constituents can be computed:

$$g_{2MS_2} = \arctan(A_m \sin g_m - A_{\mu 2} \sin g_{\mu 2})/(A_m \cos g_m - A_{\mu 2} \cos g_{\mu 2})$$

$$A_{2MS_2} = (A_m \cos g_m - A_{\mu 2} \cos g_{\mu 2})/\cos g_{2MS_2}$$

where A_m and g_m are the amplitude and the phases obtained by harmonic analysis at frequency $\omega_{\mu 2}$, ie ω_{2MS_2}.

2) THE $3MSN_2$ AND SNM_2 WAVES

These constituents, due to nonlinear interactions between M_2, S_2 and N_2 (and thus impossible to avoid in the simulation) appear at frequencies close to the N_2 constituent, and the $L_2 + 2MN_2$ group, respectively, introducing a modulation of these main constituents with a period of approximately 200 days. Over one month of simulation, it is impossible to separate them by the harmonic analysis method.

The $3MSN_2$ constituent, however, must be of small amplitude. By reference to harmonic analysis results of *in situ* observations in the Channel over one year we can estimate the amplitude of that nonlinear constituent of the order of 5% of N_2. Thus, the solution of the present numerical simulation may involve for N_2 a possible error of that order.

The amplitude of the SNM_2 constituent can be estimated of the same order as the nonlinear $2MN_2$ wave. As we can define the characteristics of the astronomical constituent L_2 in the same way as presented just before (cf. μ_2), the nonlinear contribution of $2MN_2$ and SNM_2 to that frequency can be derived as before, and we state that it must be approximately the sum of the two

$$A_{NL} \cos(\omega_{L_2} t - g_{NL}) = A_{2MN_2} \cos(\omega_{L_2} t - g_{2MN_2}) + A_{SNM_2} \cos(\omega_{L_2} t - g_{SNM_2}).$$

Taking, by reference to *in situ* observation, the extra relations

$$A_{2MN_2} = 1.3 A_{SNM_2}, \quad g_{2MN_2} = g_{SNM_2}$$

it is possible to deduce the approximate amplitudes and phases of these nonlinear constituents.

3) ANALYSIS OF THE RESIDUALS

The harmonic analysis of the computed signals are thus based on the 24 constituents selected in Section 5a and introduced at the marine boundaries of the model. It is then possible to deduce the residual $\epsilon(t)$ of formula (14), which include the numerical noise, and the nonlinear components generated inside the domain but ignored in the analysis. Three typical spectra of $\epsilon(t)$ are presented in Fig. 9. Most of the spectra are similar to Fig. 9a, with very low noise (less than 5 mm), having weak peaks at typical frequencies which are linear combinations of the main generating frequencies.

In Le Havre, where it is *a priori* known that the tide is very nonlinear, the spectrum of the residual appears to have very significant extra constituents, such as the height diurnal M_8 with a period of 3 h 06 min and an amplitude of 5 cm.

In the Bay of Mont St Michel (St Malo), an increase of the numerical noise is observed in the spectra between periods of 4 h to 10 h, which perhaps can be related to the very shallow depths in that area. A significant peak also can be noticed at 8 h 12 min, with an amplitude of 3 cm, which can be interpreted as the first harmonic interaction between M_2 and K_1.

Globally, the very low noise and the few number of extra waves observed in these residual spectra produce confidence in the results of the simulation. We critically analyze them in the following paragraphs.

6. Analysis of the results for the sea surface elevation

From the harmonic analysis of the ζ data, cotidal and corange maps for the 24 constituents have been obtained for the English Channel. Since it is impossible to present all of these results, we shall limit the presentation to some typical constituents.

a. The semidiurnal astronomical constituents

The M_2 solution obtained through the present simulation is exactly the same as the one presented in Fig. 5, and commented on Section 4d. This confirms the accuracy of the damping value established on Section 5b.

Results for the other semidiurnal astronomical constituents S_2, N_2, μ_2 and L_2 are qualitatively similar to the M_2 solution. As an illustration, the S_2 wave is presented in Fig. 10a. If compared to *in situ* data (see Table 2) or to the Ch-LP solutions, the present semidiurnal astronomical constituents appear to be quite good in phase, but overdamped by about 7% in amplitude. These results are somewhat disappointing. Complementary simulations, however, have led to the conclusion that there is no other possible compromise with the present model if we want to keep M_2 correct. It is difficult to clearly understand the reason why too strong differential damping affects the secondary waves.

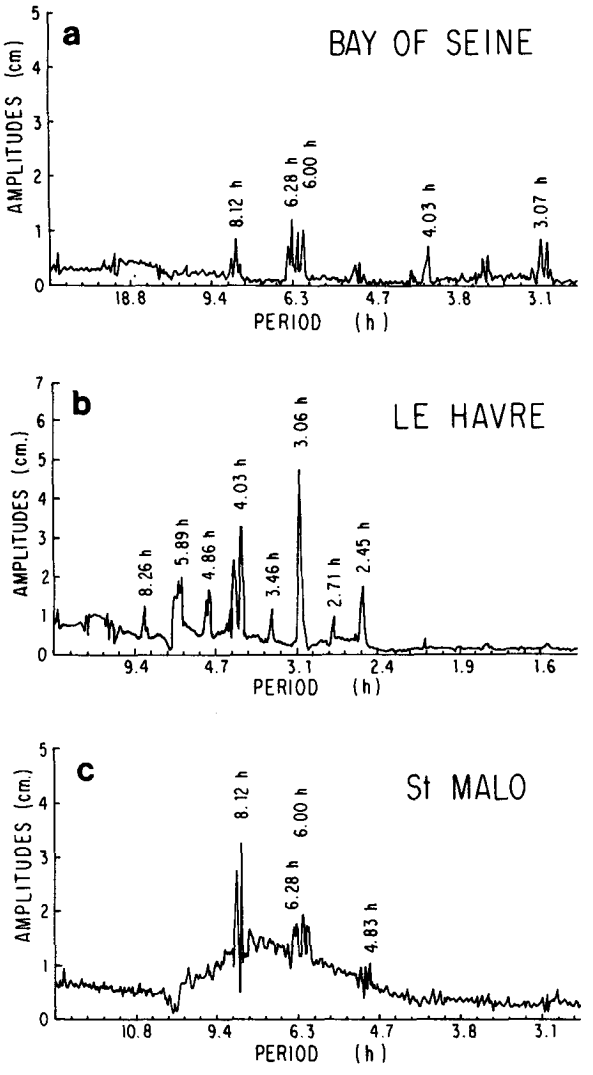

FIG. 9. Typical spectra of the residual elevation signals. Numerical noise and significant constituents not included in the analysis.

Part of it can be explained by the absence in the present simulation of semidiurnal constituents K_2, T_2, λ_2, ν_2 and $2N_2$. From relation (13), their contribution to the damping can be estimated as

$$\frac{0.75}{A_{M_2}^2}\{A_{K_2}^2 + A_{T_2}^2 + A_{\lambda_2}^2 + A_{\nu_2}^2 + A_{2N_2}^2\} \approx 0.015.$$

However, an excess of 5% remains, which cannot be a numerical bias because other authors (Pingree and Griffiths, 1981) have noticed the same problem with a model based on the same equations but using a different numerical algorithm and covering the whole North West European shelf. The quadratic bottom law used in (1) is probably nonsatisfying and needs to be modified for better results, as suggested by Pingree (1983).

b. The diurnal astronomical constituents

As an example of diurnal solutions, the K_1 tide is presented in Fig. 11. Because of its period, 23 h 56 min, its wave length is twice that of the semidiurnals, and thus its amphidromic point is located in the Strait of Dover. This feature is valid also for the other diurnal constituents O_1 and Q_1.

Qualitatively, these results are comparable to the solutions of Ch-LP and those of Pingree and Griffiths (1982). However, the amplitudes appear to be a little too high (by about 10%). That discrepancy seems to be due to the boundary value used at Roscoff [the BHI data (9.1 cm) is quite different from that used by Ch-LP (7 cm) and by Pingree and Griffiths (8 cm)]. The cotidal maps, on the other hand, are very close to the observed *in situ* values, with a standard deviation of only 6°.

c. The semidiurnal nonlinear constituents

As expected from the theory, significant semidiurnal nonlinear constituents are found in the simulated signal. In order to examine the intensity of these constituents, we note their maximum amplitude in the Bay of Mt St Michel:

$2MS_2 = 25$ cm, $2SM_2 = 9$ cm, $2MN_2 = 12$ cm

$SNM_2 = 9$ cm, $MSN_2 = 8$ cm, $MNS_2 = 8$ cm.

We already know from Ch-LP results that these waves are typically different from the semidiurnal astronomical constituents. They have a real amphidromic point in the middle of the English Channel. The MSN_2 solution is presented in Fig. 10b to illustrate this class of waves. This particular component has been chosen to show the coherence of the results for even very complex triad wave–wave interactions. The present results can be compared favorably with *in situ* observations (Table 2) and with the atlas of Ch-LP. The only important discrepancies are relative to the $2MS_2$ constituent, whose amphidromic point probably must be near the center of the domain, at the latitude of 50°N rather than at 50°30'N as here. The incorrect location of that amphidromic point introduces in our numerical $2MS_2$ solution a systematic bias over all the eastern part of the basin. However, globally, we can consider that these results are significantly realistic. If we also recall that the main source of these components is the bottom friction (Le Provost, 1976), it must be expected that a better parametrization of the quadratic law used in (1), already suggested from the unsatisfactory results of the semidiurnal astronomical constituents, will improve these nonlinear semidiurnal solutions.

d. The quarter-diurnal constituents

The M_4 solution obtained by the present simulation is exactly the same as the one presented in Fig. 6.

TABLE 2. Amplitudes A (cm) and phases g (deg in parentheses) of the main constituents. Comparison with *in situ* data along the coasts.

A (cm) g (°)	St Malo		Cherbourg		Le Havre		Dieppe		New Haven		Nab Tower		Portland	
	Observed	Model	Observed	Model	Observed	Model	Observed	Model	Observed	Model	Observed	Model	Observed	Model
Semidiurnal astronomical														
M_2	374 (178)	368 (174)	187 (230)	191 (228)	261 (284)	264 (279)	308 (311)	308 (307)	222 (320)	219 (312)	144 (317)	152 (314)	63 (194)	66 (192)
S_2	147 (229)	135 (225)	69 (273)	67 (273)	88 (331)	83 (327)	102 (1)	95 (358)	72 (8)	66 (3)	45 (1)	46 (2)	32 (243)	32 (242)
N_2	74 (162)	66 (162)	36 (210)	34 (212)	48 (265)	44 (264)	57 (291)	52 (290)	41 (297)	38 (298)	29 (285)	27 (298)	15 (184)	13 (184)
μ_2	11.5 (134)	11.5 (152)	5.7 (195)	5.4 (196)	8.1 (249)	7.0 (251)	9.4 (273)	8.2 (277)	6.8 (277)	6.0 (285)	4.4 (277)	4.2 (286)	1.9 (175)	2.0 (177)
L_2	10.5 (194)	9.7 (186)	5.2 (246)	5.0 (244)	7.2 (300)	6.4 (295)	8.5 (327)	7.5 (323)	6.2 (336)	5.6 (327)	4.0 (333)	4.0 (329)	1.7 (200)	1.8 (200)
Semidiurnal nonlinear														
$2MS_2$	25 (234)	22.5 (235)	4 (283)	7 (300)	10 (23)	14 (10)	15 (46)	19 (40)	10 (61)	12 (45)	5 (89)	7 (45)	9 (190)	7.5 (200)
$2SM_2$	8.5 (31)	7.9 (36)	2 (105)	2.6 (96)	5 (184)	4.4 (163)	7 (208)	5.8 (198)	3 (195)	3.3 (205)	3 (221)	1.8 (208)	1.5 (356)	2.2 (25)
$2MN_2$	10.3 (319)	10 (317)	2.7 (2)	3.4 (50)	5.6 (87)	7.0 (107)	9.5 (111)	9.3 (130)	6.2 (116)	6.2 (136)	2.9 (153)	3.4 (148)	3.1 (260)	3.4 (277)
MSN_2	6.6 (23)	6.3 (10)	1.6 (23)	2.7 (80)	4.0 (161)	4.7 (133)	5.0 (184)	5.4 (167)	2.7 (196)	3.2 (167)	2.0 (192)	1.9 (162)		
MNS_2	5.0 (220)	6.1 (215)	0.4 (280)	2.7 (273)	3.2 (26)	4.4 (329)	4.8 (43)	4.8 (0)	2.9 (43)	2.8 (355)	1.8 (75)	1.9 (344)		
SNM_2	4.7 (319)	8.0 (317)	2.7 (2)	2.6 (50)	4.5 (87)	5.4 (107)	7.2 (111)	7.2 (130)	4.4 (116)	4.8 (136)	1.4 (153)	2.6 (148)	1.7 (260)	2.6 (277)
Diurnal														
K_1	9.3 (36)	11.2 (94)	9.0 (106)	10.9 (110)	9.6 (119)	11.4 (124)	7.5 (123)	10.2 (130)	7.5 (108)	9.3 (120)	9.3 (113)	9.8 (122)	9.8 (113)	9.7 (118)
O_1	7.9 (344)	9.1 (348)	6.4 (354)	6.9 (6)	5.6 (9)	6.1 (27)	4.1 (36)	5.2 (50)	2.7 (323)	2.2 (45)			5.3 (344)	4.9 (0)

						Quarter-diurnal										
M_4	28 (279)	27 (235)	15.5 (353)	14.5 (354)	24.5 (75)	25 (73)	26 (185)	26 (178)	9.5 (242)	7 (233)	15 (354)	11.5 (343)	12.5 (30)	14 (16)		
MS_4	21 (335)	25 (346)	8 (49)	8.4 (47)	16 (130)	17 (127)	17 (242)	16 (234)	5 (293)	3.4 (290)	10 (51)	7.0 (47)	7.5 (82)	7.4 (76)		
MN_4	11.1 (267)	12.9 (280)	4.5 (334)	5.0 (336)	8.1 (54)	9.0 (56)	9.3 (162)	9.0 (163)	3.3 (214)	2.2 (220)	3.8 (331)	4.0 (328)	5.1 (7)	4.7 (2)		
						Sexto-diurnal										
M_6	2.5 (352)	1 (339)	2.5 (101)	3.5 (90)	15.2 (286)	17.9 (262)	3.0 (299)	3.6 (320)	2.0 (160)	1.5 (106)	4.0 (119)	4.4 (92)	6.0 (63)	6.5 (52)		
$2MS_6$	3 (39)	2 (55)	3 (135)	3.5 (128)	15 (331)	15.1 (309)	2 (351)	3.4 (338)	2.5 (196)	0.9 (209)	6.5 (166)	4.6 (130)	6.0 (109)	6.1 (100)		
$2MN_6$	1.9 (311)	1.0 (322)			10.6 (247)	8.0 (253)					2.9 (95)	1.3 (21)	4.4 (38)	3.9 (42)		

This is not surprising, when we remember that its production involves only the M_2 constituent, at least at the second order of approximation.

But we obtain now, through the interactions between M_2 and S_2, M_2 and N_2, nonlinear waves such as MS_4 (presented in Fig. 10c) and MN_4, which look very similar to M_4. It can be notice that, in good agreement with theory (Le Provost, 1974), their amplitudes are in the ratio of the intensity of the generating constituents, and their phases in relation:

$$M_4/MS_4 = 1.5 \Leftrightarrow A_{M_2}{}^2/2A_{M_2}A_{S_2} = 1.45$$

$$g_{M_4} - g_{MS_4} = -55° \Leftrightarrow g_{M_2} - g_{S_2} = -50°$$

$$M_4/MN_4 = 2.9 \Leftrightarrow A_{M_2}{}^2/2A_{M_2}A_{N_2} = 2.75$$

$$g_{M_4} - g_{MN_4} = +15° \Leftrightarrow g_{M_2} - g_{N_2} = 16°.$$

These quarter-diurnal solutions are very close to the observations. When compared with *in situ* data, the standard deviation in amplitude and phase of these solutions are

1.3 cm and 13° for M_4 (maximum amplitude 43 cm)

1.6 cm and 5° for MS_4 (maximum amplitude 39 cm)

1 cm and 5° for MN_4 (maximum amplitude 20 cm)

e. The sexto-diurnal constituents

Remember that the M_6 constituent obtained from the M_2 simulation alone was non-satisfying (by about 35%). The M_6 solution issuing from the present simulation appears very satisfactory (cf. Fig. 12 and Table 2). This confirms the idea developed by Le Provost (1974) concluding from developments (9) that the secondary waves contribute at the order A_j^2 to the generation of that M_6 component.

The $2MS_6$ solution is presented in Fig. 10d as an illustration of that class of waves. The maximum amplitude of these components are located in the Bay of Seine, as described in Section 4d. The maximum values for the main constituents are M_6 = 17 cm, $2MS_6$ = 17 cm, $2MN_6$ = 9 cm and MSN_6 = 2.5 cm. These cotidal maps are in good agreement with the Ch-LP solutions, and *in situ* observations (standard deviation of 0.8 cm and 26° for M_6; 0.9 cm and 16° for $2MS_6$ and $2MN_6$).

7. Analysis of the results for tidal currents

The harmonic analysis of the west–east (u) and south–north (v) components of the computed velocity field leads to characteristic maps of the main velocity constituents. Some of these results are already known (for the major constituents M_2, S_2, ...) but not for the harmonic and interaction constituents. It is thus interesting to carefully analyze and compare the present solutions with *in situ* observations.

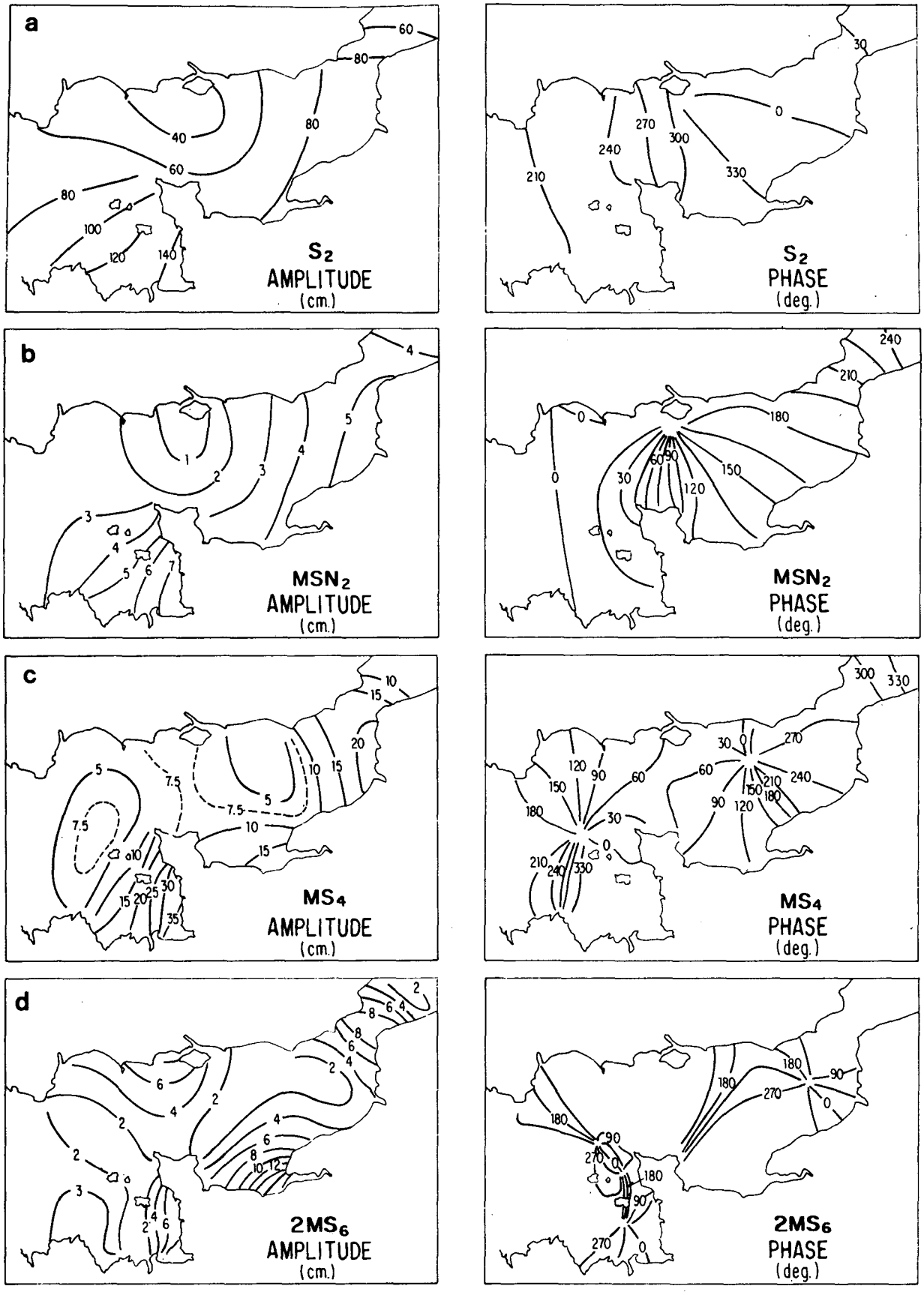

FIG. 10. Tidal amplitude and phases g (deg) for some constituents (a) semidiurnal astronomical S_2, (b) semidiurnal nonlinear MSN_2, (c) quarter-diurnal MS_4, (d) sexto-diurnal $2MS_6$.

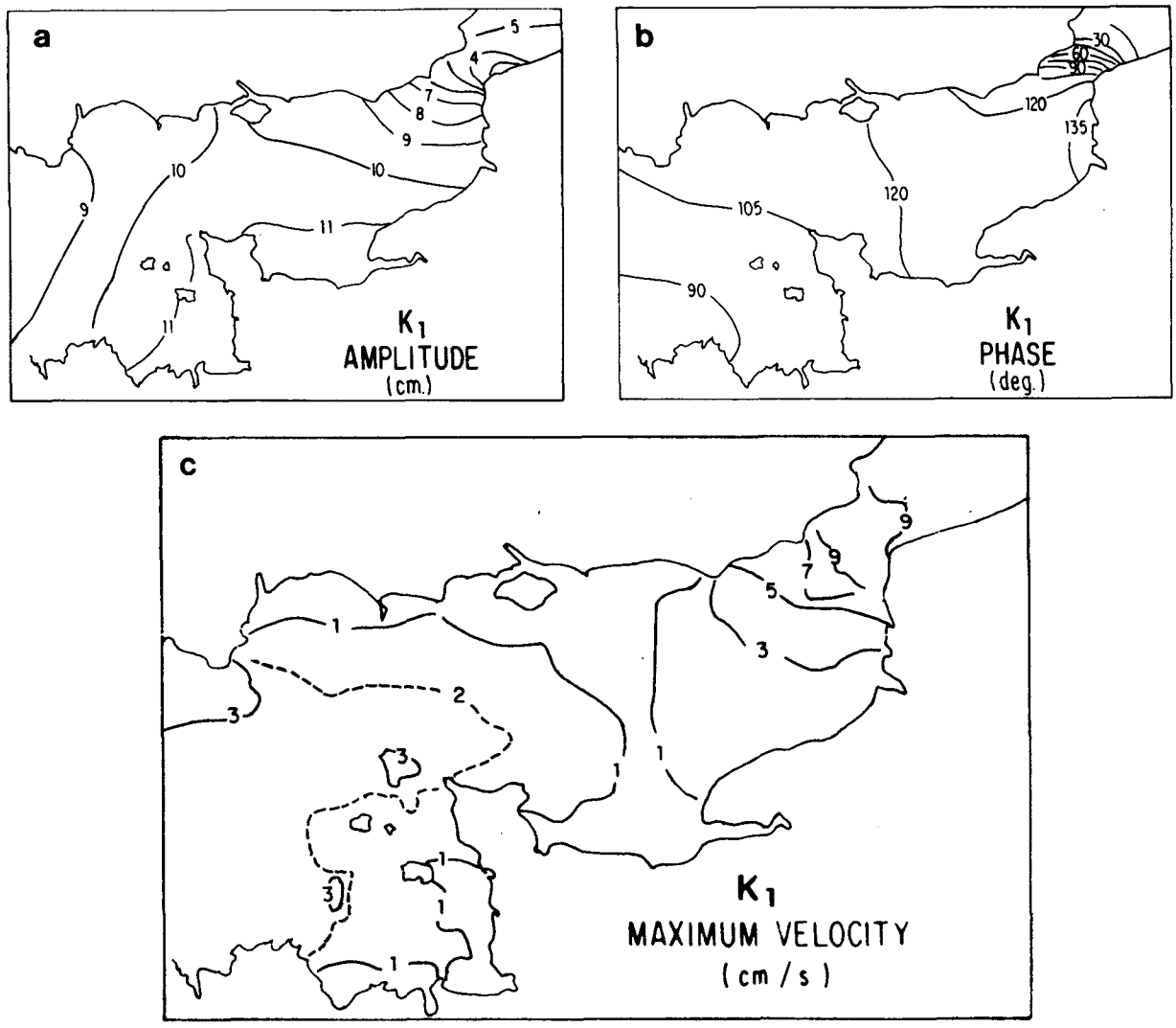

FIG. 11. As in Fig. 5 but for diurnal K_1 solution.

Four parameters are necessary to describe the velocity field: maximum velocity amplitude, direction, phase and ellipticity.

a. The semidiurnal astronomical constituents

As for the sea surface elevations, the characteristics of the different astronomical velocity components look very similar. The M_2 maximum amplitude map is presented in Fig. 5 as an illustration. The maximum velocity occurs near La Hague Cape; 208 cm s^{-1} (M_2), 63 cm s^{-1} (S_2), 33 cm s^{-1} (N_2), 5 cm s^{-1} (L_2 and μ_2); where very important gradients and rapid changes in direction are observed. In the central part of the domain, which corresponds to a nodal zone for the elevations, the velocities are large, in agreement with the Kelvin amphidrome scheme. Local maxima are also noticed between Brehat Island and Guernesey, (which is also a nodal line coupled with amplification of the tidal wave in the Bay of Mont St Michel) and in the Strait of Dover (because of the narrowness of the connection between the English Channel and the North Sea).

It is not easy to quantitatively check these results because very few harmonic datasets from *in situ* observations are available. We have used four collections of data from long-time current meter records at points P_1, P_2, P_3 and P_4 located in Fig. 2. The comparisons of the numerical results with these data are presented in Table 3. They are in very good agreement (mean deviation of 4 cm s^{-1} (M_2), 2.5 cm s^{-1} (S_2), and 3.5 cm s^{-1} (N_2) for the maximum of velocity; 4° (M_2 and S_2), and 5° (N_2) for the phases and 6° (M_2), 8° (S_2) and 3° (N_2) for the direction of the maximum velocity). The only noticeable discrepancy is on the ellipticity at points P_1 and P_4 where

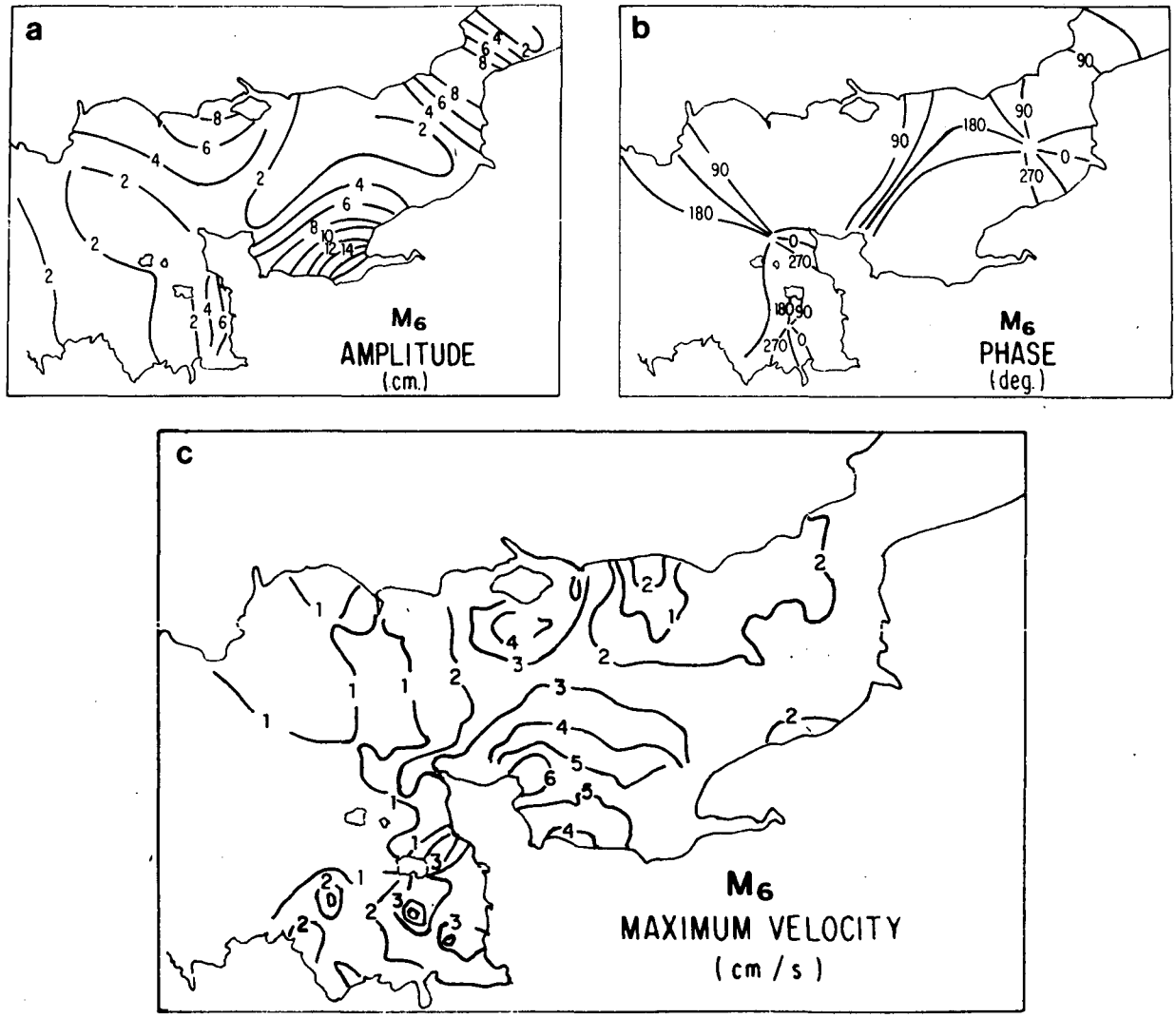

FIG. 12. As in Fig. 5 but for sexto-diurnal M_6 solution.

the sense of rotation of the velocity vector seems to be inverted. Globally, these results appear surprisingly good, given the size of the computational mesh and the complexity of the tidal current fields.

b. The semidiurnal nonlinear constituents

The networks relative to these waves do not differ much from the semidiurnal astronomical, except in the very shallow water area of the Bay of Mont St Michel, where phases are quite constant. These similarities are not surprising because of their closeness in frequency and the already observed similarities of their elevation networks. The differences observed in the shallow areas are related to the local transfer of energy towards these frequencies through friction processes.

The maximum amplitudes for these constituents are situated in the Strait of Dover and around La Hague Cape: $2MS_2$ = 15 cm s^{-1}, $2MN_2$ = 9 cm s^{-1}, MSN_2 = 5 cm s^{-1}, MSN_2 = 4 cm s^{-1} and $2SM_2$ = 3.5 cm s^{-1}.

c. The diurnal constituents

Maps of maximum amplitude, direction, phase and ellipticity for the K_1 tidal currents are presented in Fig. 12 as an illustration of the diurnal constituents. Their maxima are located in the Strait of Dover, in the area of their diurnal amphidromic point for sea surface elevation: K_1 = 13 cm s^{-1}, O_1 = 12 cm s^{-1} and Q_1 = 3.4 cm s^{-1}. It is interesting to recall that, over the same area, the semidiurnal M_2 velocities are typically 120 cm s^{-1}, i.e., only ten times the diurnal K_1. Some diurnal anomaly is probably noticable in the velocity field in the Strait of Dover. Unfortunately, we have no *in situ* observation for comparison.

d. The quarter-diurnal constituents

We know from Section 6d that the quarter-diurnal waves have two real amphidromic points in the Channel. By reference to the classical Kelvin amphidromic solution, two areas of maximum velocity amplitude must be observed at the longitude of these sea surface amphidromes, with a minimum in between. The maximum values for the main constituents of that species are effectively obtained:

between Brehat and Guernesey (M_4 = 18 cm s^{-1}, MS_4 = 14 cm s^{-1}, MN_4 = 7 cm s^{-1})

between New-Haven and Fecamp (M_4 = 15 cm s^{-1}, MS_4 = 9 cm s^{-1}, MN_4 = 5 cm s^{-1}).

As an illustration of the quarter-diurnal networks, we present the M_4 solution in Fig. 6. It is also interesting to point out in Table 3 an increase of ellipticity of the velocity in the areas of minimum amplitude, in the central part of the Channel, and near the eastern coast of the basin. This seems to be confirmed by *in situ* data, at least at point P_1, where the quarter-diurnal amplitudes, although small, are however significantly out of the noise.

The comparisons with the *in situ* data of Table 3 are surprisingly good for points P_1 and P_2.

e. The sexto-diurnal constituents

Significant amplitudes are obtained for these waves between the Bay of Seine and The Isle of Wight, in agreement with the transverse oscillation observed on the cotidal networks (M_6 = 8 cm s^{-1}, $2MS_6$ = 7 cm s^{-1}, $2MN_6$ = 3 cm s^{-1}).

The M_6 solution is presented in Fig. 12; the comparison with observations at points P_1 and P_4 brings some confidence to these results in the area of significant amplitude. Of course, outside that central zone of the Channel, all the details presented are unrealistic.

f. The long-period constituents

It is now well known that nonlinear tidal distorsions produce transfers of energy not only toward the higher but also toward the lower frequencies, inducing tidal residuals. From the present monthly simulation, residual currents have been identified, with semi-monthly and monthly modulations corresponding, in the tidal spectrum, to the mean value, and the components MS_0 and MN_0 (coming from the nonlinear transfer of energy between M_2 and S_2, and M_2 and N_2).

Although these results are impossible to validate because it is quite impossible to identify these long-term variabilities in the current meter observations, we present in Fig. 13 the residual velocity field produced by our simulation since it shows several very coherent patterns. The existence of several eddies related to the topography of the coastline can be observed, with local intense residual velocities up to 10–20 cm s^{-1}. Similar results have been produced and intensively analysed by Pingree and Maddock (1977), who showed several recent observations on sediment transports, and satellite pictures on turbidity which seem to confirm these coherent structures.

The present monthly simulation has the ability to generate the long-period MS_0 and MN_0 constituents, which modulate the intensity and the direction of these residual currents over 15 and 29 days. The intensity of these constituents are significant in the areas where the residual current is itself important;

Barfleur Cape R.C.:

24 cm s^{-1}, MS_0 = 11 cm s^{-1}, MN_0 = 5 cm s^{-1}

La Hague Cape R.C.:

13 cm s^{-1}, MS_0 = 6 cm s^{-1}, MN_0 = 3 cm s^{-1}

Brehat Island R.C.: 5 cm s^{-1}, MS_0 = 3 cm s^{-1}.

These results indicate that, at some periods, the residual currents must be reduced to a very low value, or enhanced to nearly double their mean.

The main origin of these long-period phenomena is the effect of nonlinear advection, important in areas of large velocity gradients and curvatures of the velocity field. This occurs particularly around capes. It is difficult to insure that these results are quantitatively correct, because of the lack of *in situ* bench marks. However, we have noticed previously the good agreement of our results with observations, for the quarter-diurnal components, which are produced by the same nonlinear processes as these residuals. We think consequently that some confidence can be given to the present results.

8. Conclusions

The main goals of this paper were to present a long-time numerical simulation of the tides within the English Channel and to investigate the ability of such a simulation to correctly reproduce the nonlinear processes distorting the tidal waves when propagating in shallow water areas. In order to be able to correctly analyze the results through a classical harmonic analysis approach, a monthly simulation involving 24 constituents has been realized. Particular care has been devoted to open boundary condition specifications, in order to fit them as closely as possible to reality and to enable comparison of the different numerical harmonic solutions with available *in situ* data. The English Channel was selected as a test area because the tides are well documented there, from extended analysis of numerous *in situ* observations, and from several investigations published in the literature.

TABLE 3. Amplitude, phase, ellipticity and direction of the main tidal velocity constituents, at points P_1, P_2, P_3 and P_4 (for location see Fig. 2). Comparison with *in situ* data.

	P_1		P_2		P_3		P_4	
	Observed	Model	Observed	Model	Observed	Model	Observed	Model
Semidiurnal astronomical constituents								
M_2								
Amplitudes (cm s^{-1})	96.2	92	81.6	83	155.2	157.5	150.4	142.0
Phases (deg)	33	33	59	58	226	216	218	201
Ellipticity (% × 100)	4	−6			3	2	3	−7
Direction (deg/North)	312	300			79	84	89	91
S_2								
Amplitudes (cm s^{-1})	28.9	29	23.4	25.9	47.5	50.0	39.0	44.0
Phases (deg)	78	82	285	288	271	264	253	249
Ellipticity (% × 100)	−8	−8			3	2	9	−7
Direction (deg/North)	310	301			77	84	84	91
N_2								
Amplitudes (cm s^{-1})	16.9	14.8	13.3	13.6	18.5	25.8	27.5	22.6
Phases (deg)	14	15	218	216	187	198	177	183
Ellipticity (% × 100)	4	−6			2	2	13	−7
Direction (deg/North)	298	299			77	84	79	91
Quarter-diurnal constituents								
M_4								
Amplitudes (cm s^{-1})	6.2	5.0	11.4	12.1	2.8	1.9	10.2	3.5
Phases (deg)	168	170	114	98	280	329	349	323
Ellipticity (% × 100)	−57	−52					4	−2
Direction (deg/North)	340	326					43	85
MS_4								
Amplitudes (cm s^{-1})	4.0	3.5	7.4	7.6			2.6	2.6
Phases (deg)	32	36	171	155			3	12
Ellipticity (% × 100)	−20	−38					19	−20
Direction (deg/North)	171	150					49	85
MN_4								
Amplitudes (cm s^{-1})	2.1	1.7	3.8	4.2			2.2	1.3
Phases (deg)	34	329	75	79			275	123
Ellipticity (% × 100)	28	48					18	
Direction (deg/North)	112	148					25	85
Sexto-diurnal constituents								
M_6								
Amplitudes (cm s^{-1})	5.6	5.7					4.1	3.5
Phases (deg)	173	161					172	129
Ellipticity (% × 100)	14	12					46	−8
Direction (deg/North)	135	139					93	91

TABLE 3. (*Continued*)

	P_1		P_2		P_3		P_4	
	Observed	Model	Observed	Model	Observed	Model	Observed	Model
$2MS_6$								
Amplitudes (cm s^{-1})	7.2	5.0					2.1	2.9
Phases (deg)	39	24					88	173
Ellipticity (% × 100)	5	9					52	−10
Direction (deg/North)	326	316					98	90
$2MN_6$								
Amplitudes (cm s^{-1})	2.2	2.6					2.3	1.7
Phases (deg)	6	323					136	117
Ellipticity (% × 100)	14	16					48	−7
Direction (deg/North)	296	315					96	90

From the present results, it appears that, with the class of simplified numerical model used (two-dimensional, vertically integrated, with coarse meshes), it is possible to correctly simulate quite complex tidal wave distortions. Nonlinear semidiurnal, quarter-diurnal, sexto-diurnal, and even low-frequency semimonthly and monthly constituents are surprisingly well reproduced, involving double and triple wave–wave interactions. However, the results on the main semidiurnal astronomical waves except M_2 are somewhat disappointing: they reveal real problems of damping; the classical quadratic bottom friction law seems to overdamp the secondary wave in the presence of the dominant M_2 wave. This suggest the need of better modeling of the near bottom dissipation processes. Given these imprecisions of secondary astronomical waves, one may be surprised by the quality of the nonlinear tidal solutions. This apparent paradox results from the fact that all of these nonlinear waves are issued from nonlinear processes dominated by the M_2 tide which is correctly reproduced (within 2% for the amplitudes and 5% for the currents).

With the set of harmonic parameters thus obtained, it is possible to realize predictions of water levels and

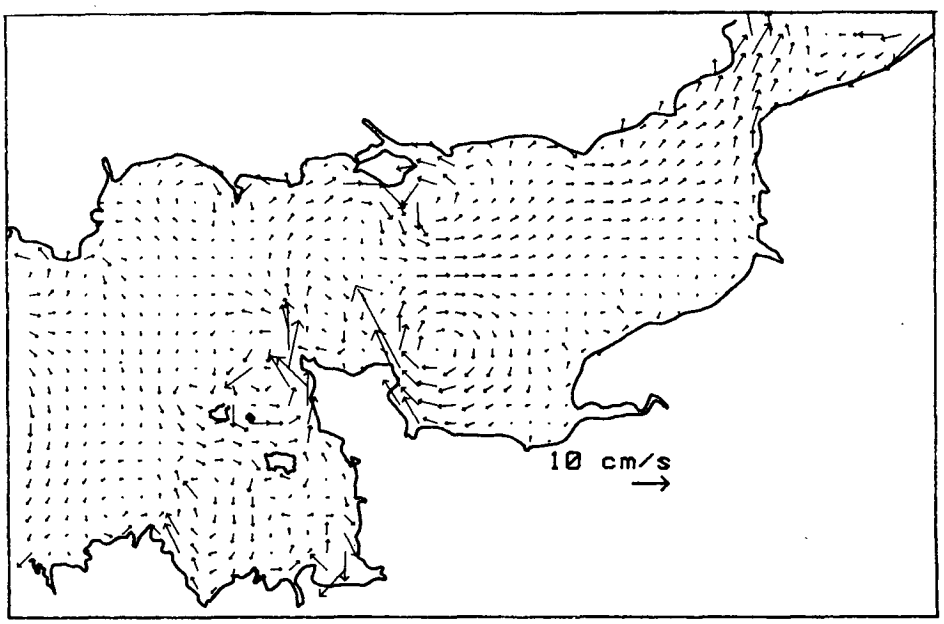

FIG. 13. Residual currents.

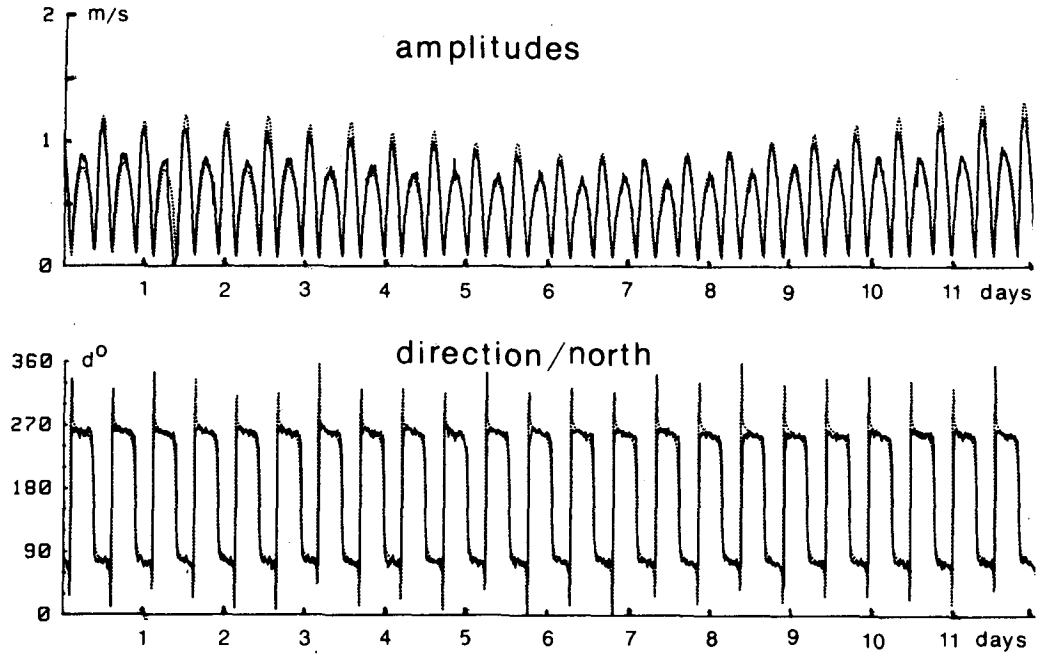

FIG. 14. Hindcast of tidal currents at point P_2. Numerical solution (dotted line) compared to observations (solid line) over 12 days, since 2200 GMT 10 December 1976.

currents, everywhere over the English Channel, in the way of the tidal predictions for harbors. An example of such a computation is presented in Fig. 14 for point P_2. It can be seen how good the prediction can be, when compared to observations. For the present case, the differences between ebb and flow are particularly well reproduced, due to the relative importance of the quarter-diurnal constituents there. Over 40 days of comparison between harmonic recomputation and observation, the standard deviation is only of 8.9 cm s^{-1} for currents approaching 1.5 m s^{-1}, with standard errors of 9° for the instantaneous direction of the velocity.

The present study demonstrates the feasibility of using classical two-dimensional numerical models to compute tides within large coastal areas, even if nonlinear effects are important, provided that 1) second order scheme is implemented, 2) a detailed tidal spectrum is considered and 3) correct boundary conditions are used. However, one important problem remains unsolved, related to the damping of the secondary waves of the spectrum, which limits the over all satisfying precision of the simulations.

Acknowledgments. This work has been supported by the National Center of Scientific Research and by the Institut Français de Recherche pour l'Exploitation des Mers under Contract 80/6260. The basic version of the numerical model used has been supplied by F. Ronday under C.N.R.S. Contract 2577. The authors thank R. L. Haney and the referees for their valuable comments.

REFERENCES

Batten, M., and J. Han, 1981: On the computational noise of finite differences schemes used in ocean models. *Tellus,* **33,** 387–396.

Bertherat, C., R. Carcel and C. Le Provost, 1981: Analyse de courants et niveaux en Baie de Seine. Institut de Mecanique de Grenoble Intern. Rep. No. 79/6041, 123 pp.

Chabert d'Hières, G., 1962: Reglage et exploitation de la plaque tournante de Grenoble. Mémoires et travaux de la SHF. La Houille Blanche, **2,** 244–254.

——, and C. Le Provost, 1979: Atlas des composantes harmoniques de la marée dans la Manche. *Ann. Hydrogr.,* **6,** 5–36.

Flather, R. A., 1976: A tidal model of the North East European continental shelf. *Mem. Soc. R. Sci. Liège,* Ser 6, **10,** 141–164.

Fornerino, M., and G. Chabert d'Hières, 1982: Etude des courants de la marée M_2 dans la Manche à l'aide du modèle réduit de Grenoble. *Ann. Hydrogr.,* **9,** 13–31.

Gallagher, B. S., and W. H. Munk, 1971: Tides in shallow water: Spectroscopy. *Tellus,* **23,** 346–363.

Godin, G., 1972: *The Analysis of Tides.* Liverpool University Press-University of Toronto Press, 264 pp.

Johns, B., 1983: Physical oceanography of coastal and shelf seas. *Elsevier Oceanography Ser.,* No. 35, 470 pp.

Kabbaj, A., and C. Le Provost, 1980: Non linear tidal waves in channel: A perturbation method adapted to the importance of quadratic bottom friction. *Tellus,* **32,** 143–163.

Kreiss, H., 1957: Some remarks about nonlinear oscillations in tidal channels. *Tellus,* **9,** 53–68.

Lamb, H., 1932: *Hydrodynamics.* Cambridge University Press, 278–282.

Le Provost, C., 1973: *Décomposition Spectrale du Terme de Quadratique de Frottement dans les Équations des Marées Littorales.* Académie Science, 571–574 and 653–656.

——, 1974: Contribution à l'etude des marées dans les mers littorales. Application à la Manche. Thèse d'état, Université de Grenoble, 228 pp.

——, 1976: Theoretical analysis of the structure of the tidal wave spectrum in shallow water areas. *Mém. Soc. R. Sci. Liège,* **6,** 91–111.

——, 1981: A model of prediction of tidal elevation over the English Channel. *Oceanol. Acta,* **4,** 279–285.

——, 1983: An analysis of SEASAT altimeter measurements over a coastal area: The English Channel. *J. Geophys. Res.,* **88,** 1647–1654.

Nihoul, J. C. J., 1975: *Modelling of Marine Systems.* Elsevier, 283 pp.

Pingree, R. D., 1983: Spring tides and quadratic friction. *Deep Sea Res.,* **30,** 929–944.

——, and L. Maddock, 1977: Tidal residuals in the English Channel. *J. Mar. Biol. Assoc. U.K.,* **57,** 339–354.

——, and ——, 1978: The M_4 tide in the English Channel derived from a nonlinear numerical model of the M_2 tide. *Deep Sea Res.* **25,** 53–63.

——, and D. K. Griffiths, 1981: S_2 tidal simulations on the northwest European shelf. *J. Mar. Biol. Assoc. U.K.,* **61,** 609–616.

——, and ——, 1982: Tidal friction and the diurnal tides on the northwest European shelf. *J. Mar. Biol. Assoc. U.K.,* **62,** 577–593.

Richmeyer, R., and K. W. Morton, 1967: *Difference Methods for Initial-Value Problems.* Wiley and Sons, 179 pp.

Roache, J. P., 1972: *Computational Fluid Dynamics.* Hermosa, 446 pp.

Ronday, F., 1977: Courants de marées et circulations résiduelles dans la Manche. Institut de Mecanique de Grenoble Intern. Rep. No. 77/2577, 20 pp.

Shureman, P., 1958: *Manual of Harmonic Analysis and Prediction of Tides.* Coast and Geodetic Survey, Special Publ. 98, U.S. Dept. of Commerce, 317 pp.